Experimental study on the optimal performance of gas turbine (GT) inlet air filtration system for offshore application

Samuel O. Effiom[1], James A. Ajor[1], Precious-Chibuzo O. Effiom[2], Isuamfon Edem[3], Paschal Ubi[4], Fidelis Abam[4*] and Ogheneruona E. Diemuodeke[5]

*Correspondence:
fidelisabam@unical.edu.ng

[1] Department of Mechanical Engineering, University of Cross River State, Calabar, Nigeria
[2] Department of Petroleum Engineering, University of Calabar, Calabar, Nigeria
[3] Department of Mechanical Engineering, Akwa Ibom State University, Ikot Akpaden, Nigeria
[4] Department of Mechanical Engineering, University of Calabar, Calabar, Nigeria
[5] Department of Mechanical Engineering, University of Port Harcourt, Choba, Nigeria

Abstract

An experimental study on the optimal gas turbine inlet air filtration system performance for offshore applications is presented. The objective is to conduct a comparative real-time data analysis for an offshore selection of optimal filtration system. Different filtration configurations were set up in a wind tunnel under simulated offshore environmental settings. The considered filter grades (A, B, C, D, E and F) align with the ASHRAE filter class (F7, H12, E11, E10, G5 and F9). Offshore contaminants weighing 1000 g, ranging between 0.05 and 20 μm, were used based on ASTM standards. The contaminants were loaded between 20 and 100% mass. The results indicate that the accumulated contaminant across the filter elements at 100% loading for A, B, C, D, and E filters ranged between 205.36 and 318.02 g. Similarly, the pressure differential change across the filters A–B, D–E, B–C, E–F, and filter housing inlet–outlet were estimated at 19.02 kPa, 16.9 kPa, 2.54 kPa, 2.86 kPa, and 2.25 kPa, respectively, while the particle removal efficiency for A, C and D filters were highest calculated at 53%, 58.22% and 51.69%, respectively. The result proved significant, with an overall improvement in the compressor output at 205 kW for a pressure change of 2.25 kPa at the filter housing outlet used to establish the optimal performance. The filter elements recorded decreased efficiency across the compressor stages due to mass accumulation on the media surface area. The study inferred that a 3-stage filtration with filter combination A–B (F7–H12), D–E (E10–G5), and B–C (H12–E11) is suitable for an inlet filtration system for GTs operating within the studied offshore environment.

Keywords: Gas turbine, Inlet filtration, Optimal filter selection, Offshore, Contaminants

Introduction

Gas turbines (GTs) have evolved over the last decade with increasing demand for power generation and other drive applications, especially in the oil downstream and off-stream sectors [1]. The offshore oil and gas sector relies greatly on power generated by GT plants to power the subsystems within the oil installations [2]. In applying GTs, the main concerns of GT users and operators are availability, reliability and maintenance costs. Effective maintenance is indispensable for high-level reliability, GTs, and maintenance approaches are imperative [3]. The performance of GT slowly deteriorates during its

Effiom *et al. Journal of Engineering and Applied Science*   (2023) 70:131

Page 2 of 18

operation, even under typical engine operating conditions [4]. Generally, GTs have different operating environments based on the site condition concerning contaminants that affect GT performance [5]. The performance of GTs in service needs to be maximised. However, to achieve this, clean and quality air ingestion into the engine is of the essence [6, 7]. Fouling, corrosion, and erosion remain prevalent factors in reducing its performance and reliability due to the clogging of filter housing [8, 9]. The offshore Environment is peculiar with pollutants from exhaust flares, leakage of oil tanks, drilling dust, paint fumes, accumulation of sea salt (SS), and hydrocarbons, which are detrimental to the GT performance [10]. Thus a suitable inlet air filter system is required to minimise the effect of these contaminants on GT performance.

Studies have shown that clogging is a major challenge that affects filter elements and housing, thus reducing engine GT performance, operability, production efficiency and life span [11, 12]. Clean inlet air filtration is indispensable to maintain GT performance, as it averts the effect of fouling, erosion, and corrosion, correlating the production capacity and longevity of GT systems [13]. The prediction of GT engine performance deterioration and clogging is highly complicated. It is challenging due to structural complexity, non-stationary operating conditions, and other uncertainties associated with GT design and environmental factors [14]. In the last few decades, scholars have kept researching alternate filtration systems/methods to mitigate the impact of contaminants on compressors and turbine blades [15–17]. Additionally, several prognostic approaches have been investigated by many researchers, and these techniques can be summed into two categories, model-based prognostics and data-driven approaches [17]. In the prognostic approach, it was observed that the rapid deterioration in the GT systems is due to the clogging of the filter housing and fouling of the surfaces of upstream sections, resulting in varying degrees of GT failures [18]. An observation from the research conducted by [19, 20] shows that some form of pollutant still enters the compressor when using three-stage filtration systems with significant clogging of the filter house**.** Unfortunately, the dynamics and complexity of the filtration system make it difficult for operators and users to maximise the power generated. The latter is because filter system design customarily comes from the original equipment manufacturers (OME). Therefore, the design process lacks a corresponding analysis of the domestic condition and running state. In practice, the environmental conditions may vary significantly as such conditions may not have been factored in during the design. The latter may impose unnecessary operation/maintenance costs and thus reduce the GT lifespan [21, 22].

Conversely, the prognostic approach has attempted different procedures. Still, it cannot be completely reliable since certain assumptions are made within its approach, which is prevalent in operations [23]. Moreover, the approach lacks experimental data from the literature to validate most of the research conducted from prognostic methods [11], which investigated the clogging trend in the filter housing of the GT engine. However, to minimise contaminants entering the compressor section and maintain the gas turbine performance, the filtration system remains a vital component to be enhanced. It should address the challenges mentioned above, ascertained by the experimental procedure. Choosing the filtration mechanism or system can be overwhelming because it involves several considerations and inputs. The filtration system selection should be based wholly on the operating philosophy and objectives for the GT, the type of contaminants existing

Effiom *et al. Journal of Engineering and Applied Science*   (2023) 70:131

Page 3 of 18

in the ambient air, the environmental peculiarity, and predictable variations in the contaminants in the future owing to momentary emission sources or periodic changes. The current study explores different filter combinations for a specific location to generate data to enhance GT production efficiency. The study adopts a pragmatic approach by using different filter classes, arrangements and selection within an experimental test rig. The study objective is to conduct a comparative real-time data analysis for an offshore oilfield that will aid in selecting an optimal filtration system for offshore applications. Such generated data are not found elsewhere as they are based on simulated contaminants within the studied oilfield. The authors have considered the study noteworthy and may form a basis for policy drive in this respect. Thus, reducing maintenance costs while extending GT life and operational time.

Methods

The materials employed include a wind test tunnel consisting of an air filter housing, filter bellmouth, filter elements, barometric total and static pressure (digital pitot tube) instrumentations, digital anemometer, centrifugal compressor (a suction mechanism), particle ingestion mechanism, digital anemometer, an electronic mixer, Labtech BL-5002 weighing electronic compact scale: salt, dust (potassium sulphate) sample, and a timer. Also, the study environment within the framework is a simulated offshore setting, characterised by high humidity contents, sea salt, hydrocarbon flare, smoke (remains of unburnt fuel as discharged from exhaust fumes and delivery vessels), and dust (blown by the wind as a result of offshore industrial activities). A flowchart of the methodology is presented in Fig. 1.

Simulated contaminant preparation

Sample test feed was obtained from a standard Laboratory facility in Nigeria. Potassium Sulphate is reported in this study as soluble test dust. The samples depicted in Fig. 2 were prepared indoors with a total measured weight of 1000 g each of salt aerosol, mist, dust, and particulate matter (PM) within the size range of 0.05 to 20 μm. This conforms to ASTM standard sample preparation for indoor testing.

Furthermore, sample weights were measured with Labtech BL-5002 digital electronic compact scale with an accuracy of ± 0.01 μg and cleansed before being meshed in B01F56/725 electronic mixer. To ensure uniform mesh, Eq. (1) was used to determine the percentage per mixture of each contaminant before testing commenced.

$$\% \, pm = 0.0053 \times M_c \tag{1}$$

where M_c is the mass concentration in submicron.

The summary of each contaminant's specifications is shown in Table 1. These samples were obtained for the experimentations because they represent the significant contaminants influencing filtration system performance within the studied offshore environs.

Test rig setup

The test rig is a wind tunnel with a centrifugal compressor as a primary drive system. The rig was modelled to resemble a typical offshore GT filtration system at the Usan oilfield, Rivers State, Nigeria. The wind tunnel test rig layout consists of different
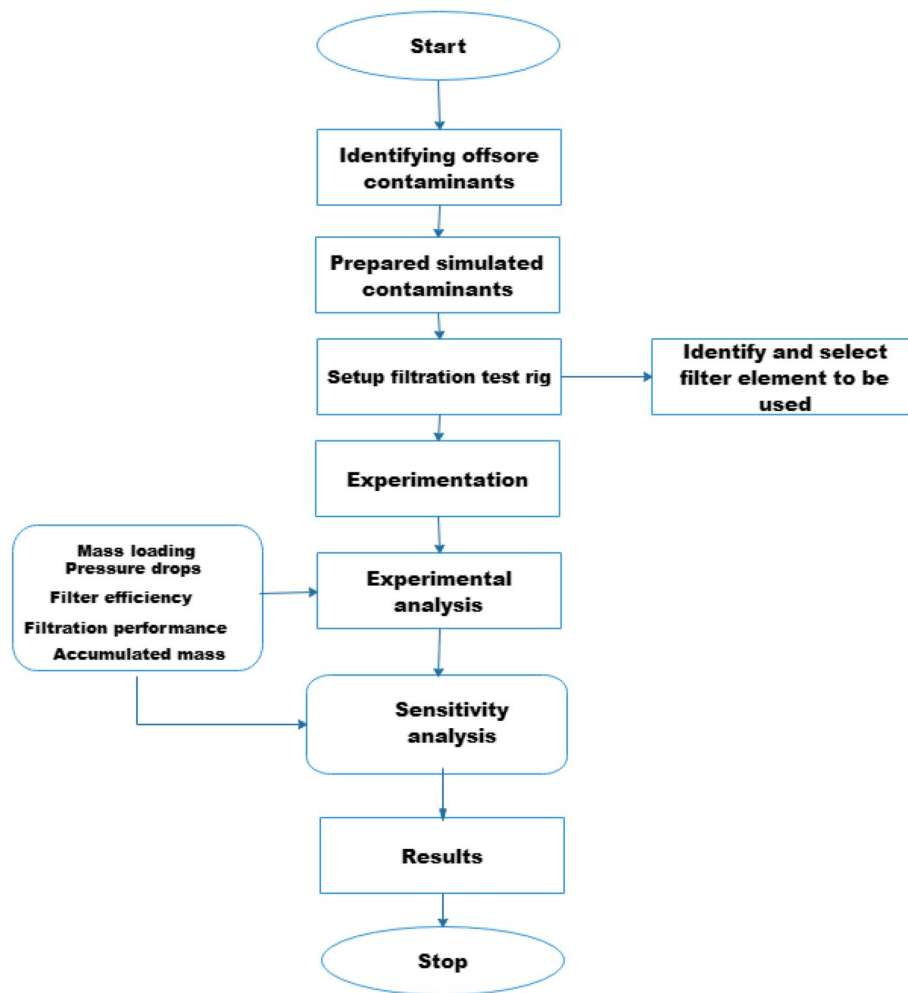
Fig. 1 Methodology flowchart

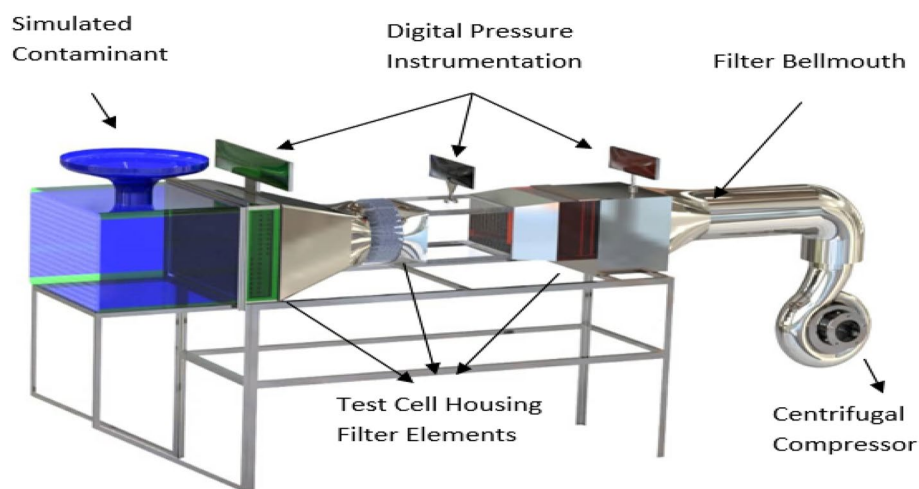**Fig. 2** Simulated contaminants sample

Table 1 Summary of simulated contaminants

Contaminants	Sample quantity (g)	Per water (ml)	% per mixture
Salt aerosol	1000	1	53
Mist	1000	1	53
Dust	1000	1	53
PM	1000	1	53

grades of filter elements arranged for various filtration system configurations in the transparent plexiglas tunnel that channels airflow at specified velocities. Barometric pressure instrumentations were also installed at different flow states of the filtration stages to measure both static and total pressures simultaneously for each test sample, as indicated in Fig. 3. The test rig also consists of a filter bellmouth of converged configuration that houses the 132–263-kW SLT300 centrifugal compressor which acts as both the suction and aerodynamic compressible performance mechanism.

The compressor is located downstream of the test rig. The speed is adjusted by a frequency converter that enables testing over a wide range of air velocities (± 15 m/s) through the filter elements. The wind tunnel accommodates a wide range of configurations and allows testing of various aspects of filter elements. The rig was set up in line with HVAC standards. The main filter-holding module was made of plexiglas to enable the operator to visually observe the filter performance during testing.

Filter studied

A combination of EPA and HEPA filters was selected to remove ingested contaminants. Understanding that the HEPA filter has a high-efficiency filtration capacity of removing particulate matter ± 0.1 μm [24]. Different grades of EPA and HEPA filter elements (A, B, C, D, E, F) in accordance with ASHRAE filter class (F7, H12, E11, E10, G5, F9) were studied, with filters A to C and D to E operating as high velocities filters (5.4–10 m/s) and low-velocity filters (3.5 m/s) respectively. The size ($12 \times 12 \times 0.75$ cm) filter elements with a face area of 144 g/cm^2 were specifically

Fig. 3 Test rig layout

Effiom *et al. Journal of Engineering and Applied Science*   (2023) 70:131

Page 6 of 18

selected to fit in the test cell. At the same time, they were varied at different contaminant loading conditions. To minimise errors, filter elements were cleansed with brine water and weight was determined before loading. Filter elements A, B, C, D, E, and F had corresponding weights of 347.1 g, 345.9 g, 341.2 g, 315.3 g, 314.5 g, and 314.8 g, respectively. The schematic layout of high and low-velocity filter elements for the filtration system studied is depicted in Fig. 4a and b, in that order. Furthermore, the filter elements were varied interchangeably while filter performance data was collected during condition monitoring. The proposed configuration was capable of removing contaminants ingression with accuracy ± 0.01 μm.

Experimentation

The units in the instrumentation were kept at the default setting while varying the velocity (5 m/s and 10 m/s) at constant atmospheric pressure (101.325 kPa) for the ingested contaminants. Filter elements were labelled A, B, C, D, E and F for easy assessment of their position in the intake configuration of the filter housing. Before the primary test began, an initial test was carried out without the filter elements to check the characteristics of air velocity, pressure, and uniformity of the flow. The velocity was measured through a digital anemometer (RSA485/0–20 m/s with precision 0.1 m/s) and pressure through the digital pitot tube (accuracy 1% reading and measurement uncertainty due to resolution 0.001 bar) installed at the inlet and outlet duct. The uniform wind velocity inside the test section was estimated as the average measured inlet velocity to the outlet velocity to be 12 m/s. The uniform air pressure of wind inside the test section amounted to 100.32 kPa. This was carried out within a time frame of 15 min. All measurements were observed by digital instrumentation illustrated in Fig. 3. To ensure steady-state conditions, each speed setting on the frequency-controlled compressor was held constant for a minimum of 6 min. Prepared contaminants percentage per mixture (% pm) was taken from the test cell and supplied into the airstream by impingement nozzles at 121 cm upstream from the test model. Two nozzles were used to ensure adequate coverage of the entire face area of the test filter without significant wetting of the air duct walls upstream from the filter element. The static and total pressure of filter elements A–B, B–C, C–D, D–E, and E–F were recorded along the instrumentation. The inlet and outlet air filter test performance data for the test housing was accounted for and analysed. An electronic mixer was used to determine the particulate matter (PM) mesh load for the prepared contaminants studied and the filtered air to the centrifugal compressor.
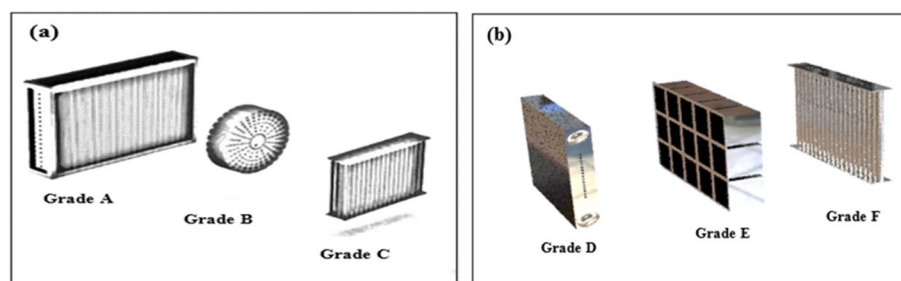

Fig. 4 Layout of filter elements studied. **a** High velocity (A, B, C). **b** Low velocity (D, E, F)

Filter element performance

The experimental result of the influence of airflow leaving inlet housing (Hi) to filter element A (Hi-A), A–B, B–C, C–D, D–E, E–F, and inlet housing to housing outlet (Hi-Ho) differentials were used to evaluate the performance characteristics of the GT under study. The specific heat ratio of air (γ), the specific heat capacity of air (Cp), air density at the inlet (ρ), and the temperature difference across compressor (ΔT) were assumed to be 1.4, 1.005 kJ/kgK, 1.2 kg/m^3, and 22.2 °C, respectively [24].

The pressure differential (ΔP_t) and filter loading efficiency (η_f) were determined from Eq. (2, 3 and 4), respectively [25, 26].

$$\Delta P_t = P_i - P_e \tag{2}$$

The accumulated mass flow (W_a) on each filter element is determined by Eq. (4) [25] as a function of the weight of tested filter elements.

$$W_a = w_m - f(A, B, C, D, E, F) \tag{3}$$

$$\eta_f = \left(\frac{W_e - W_l}{W_e} \right) \times 100 \tag{4}$$

The flow density (ρ) is obtained from Eq. (5) [27, 28]

$$\rho = \frac{P_s}{gh} \tag{5}$$

The flow rate (q) across each filtration stage is calculated from Eq. (6) [27, 29]

$$q = \sqrt{\frac{2P_t}{\rho}} \tag{6}$$

where P_t and P_s are obtained from the test instrumentations.

Furthermore, the housing intake (Hi) and outlet (Ho) parameters obtained from the experimentation were used to evaluate the compressor's performance. The performance was evaluated in terms of compressor volumetric flow rate (Q_f) and the power drawback as sensible capacity (q_s) of the compressor motor as presented in Eqs. (7) and (8), respectively [30, 31].

$$Q_f = q \sqrt{\frac{\Delta P_s}{\Delta P_t}} \tag{7}$$

$$q_s = Q_f \rho (C_P \Delta T) \tag{8}$$

Investigation of mass loading (ML) on filter elements

Mass loading of 20%, 40%, 60%, 80% and 100% ingression of particulate matter on filter elements in filter housing were investigated at intake. Performance health monitoring of filter elements involved monitoring the static and total pressure over the intake housing

using pressure instrumentations. Since the experiment did not consider variations in particle size distribution across the face area of individual filter elements, mass accumulation (W_a) was evaluated. Other performance parameters (efficiency and flow rate) were calculated from Eqs. (4) and (6), respectively. The accumulated mass flow was also evaluated from Eq. (3), whereas the weight of loaded filter elements was accounted for using Labtech BL-5002 weighing compact electronic scale.

Results and discussion

Effect of mass loading (ML) on static and total pressure

The most accumulated filter elements at 100% loading condition were recorded at intake of the filter housing. That is, A and D (318.02 g and 310.15 g). However, B, C, E, and F showed substantial contaminant mass distribution of 213.14 g, 208.14 g, 208.13 g, 205.36 g, and 199.50 g, respectively. The effects of various particulate loading (20%, 40%, 60%, 80% and 100%) on filter elements across filter housing are presented in Figs. 5, 6, 7, and 8. Figure 5 accounts for the effect of mass loading on the P_S within the stages of filtration.
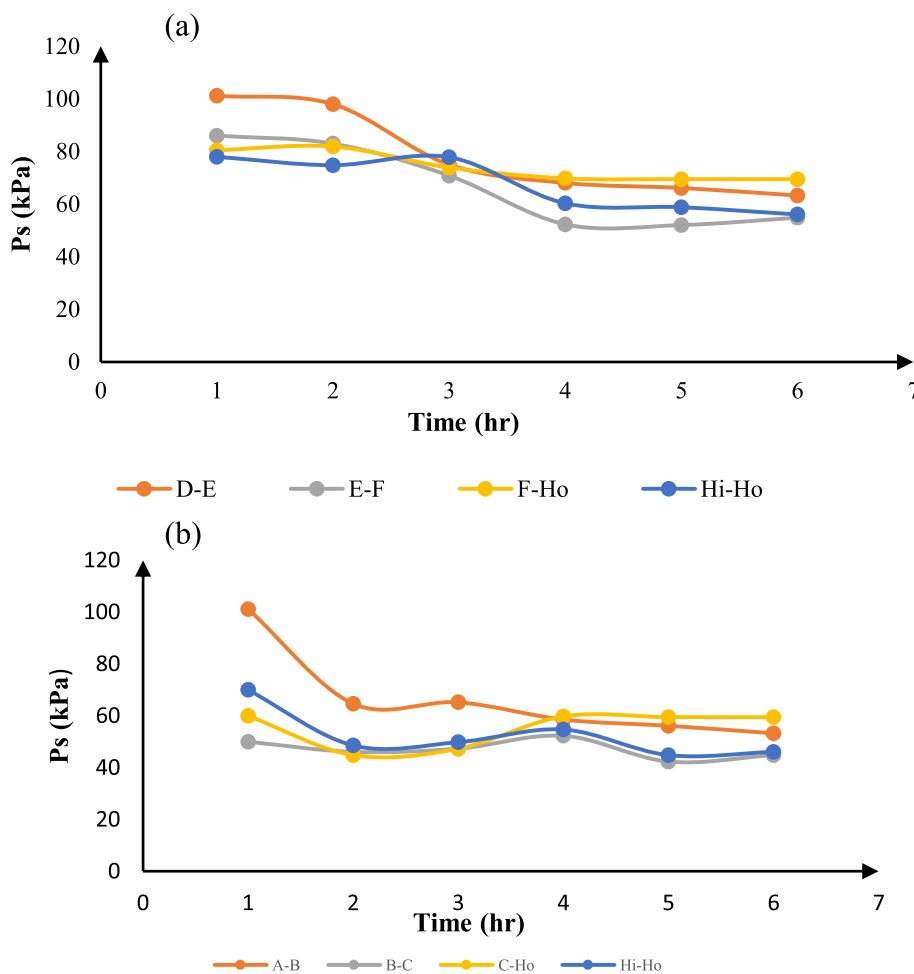

Fig. 5 **a** Static pressure at 10 m/s and **b** static pressure at 5 m/s
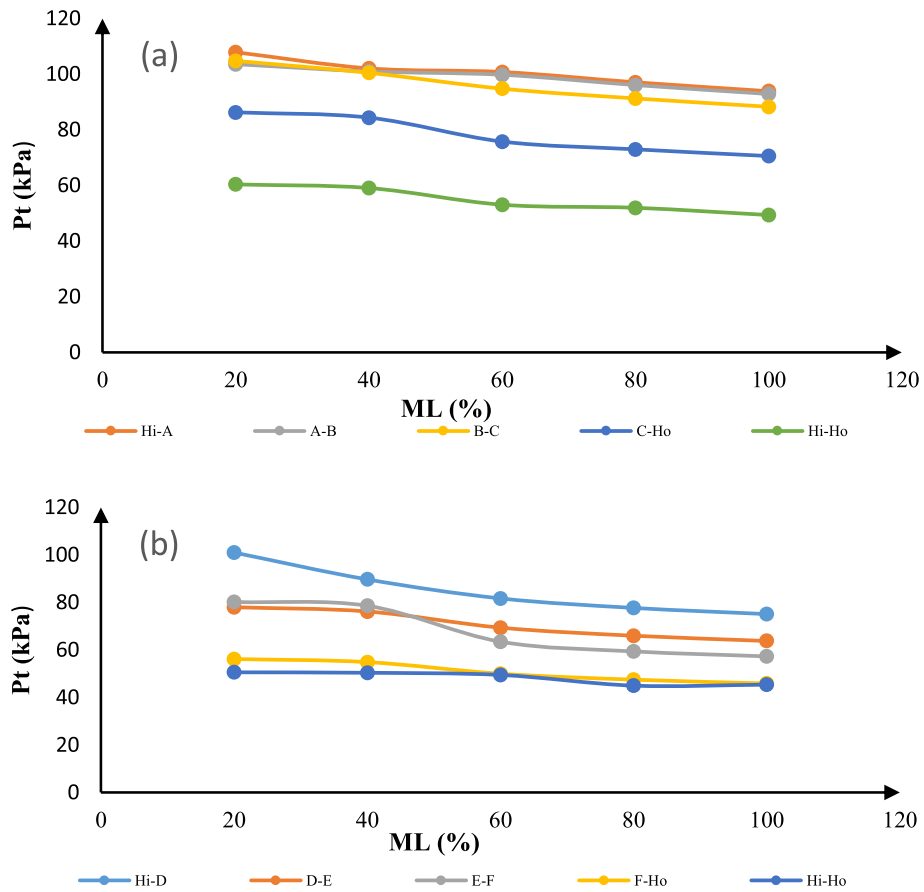
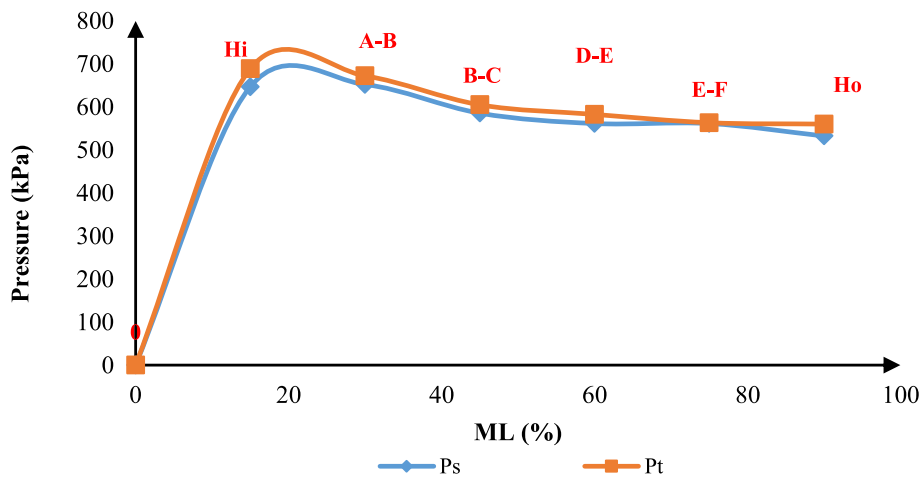**Fig. 6** **a** Total pressure at 10 m/s and **b** total pressure at 5 m/s

Fig. 7 Total pressure (P_t) vs static pressure (P_s)

From the figures, static pressure decreased at the inlet of the filter housing as contaminant concentration increased from 20 to 60%, corresponding with filter elements Hi-A, A–B, B–C, and D–E. It maintained linear correlation at 80%, 100% loading for both high
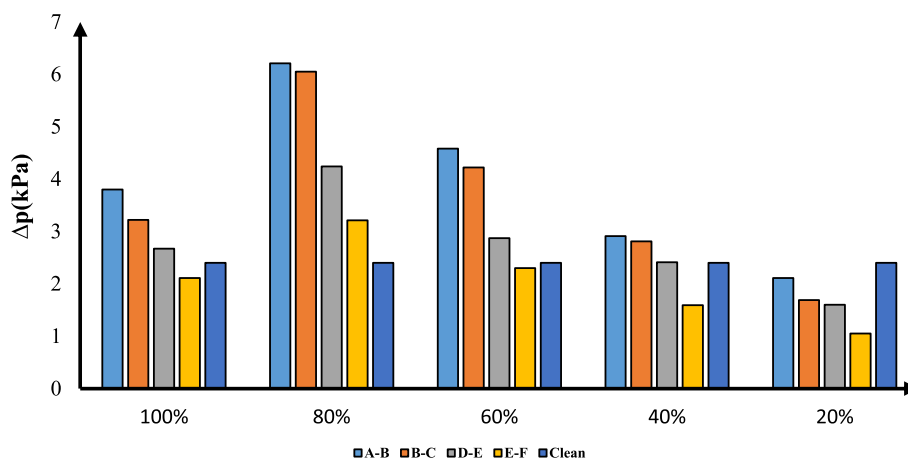
Effiom *et al. Journal of Engineering and Applied Science*   (2023) 70:131

Page 10 of 18

Fig. 8 Differential pressure (Δp) across filter housing

and low velocities, as observed in Fig. 5a and b. Similarly, Fig. 6a and b show total pressure across filter housing at various loading conditions while maintaining constant setup velocities at 10 m/s and 5 m/s, respectively.

When intercepted with filter media, the P_t across each face area of filter elements resulted in decreased pressure across the stages of filtration. However, filter combinations A–B and B–C showed higher differential (60–100% loading). In contrast, D–E and E–F showed less incremental in the differential, as discussed subsequently. The relationship between the static and total pressure is shown in Fig. 7.

Effect of mass loading on the pressure drop across filter housing

Figure 8 presents the differential pressure across the filter housing. At 80% loading condition, filter elements A–B and D–E recorded the highest-pressure differential of 6.21 kPa and 6.05 kPa, respectively, when contaminants were ingested. The pressure differential across the housing resulted from the ingested contaminant into the impingement nozzle along the flow path captured by the filter media. However, within the two velocities considered, the overall pressure differential (Hi-Ho) recorded 1.05 kPa less than B–C and E–F filtration stages with 4.24 kPa and 2.827 kPa, respectively. This result was validated by the studies of [32].

Effect of mass loading on filter elements

The effect of ML is reported in terms of mass accumulated on the surface area of filter elements A, B, C, D, E and F. This accounts for the changes in airflow as the filters attained maximum holding capacity operating at varied speeds (5 m/s, 10 m/s). Figure 9 shows how particulate matter is distributed in each varied stage of the filtration housing. The filter elements showed particulate deposition at each varied stage. All filter elements showed decreased inlet mass flow across the filtration stages within the filter housing. However, filter elements A and D at 80% to 100% loading showed maximum accumulation of 318.02 g and 310.15 g, respectively, while maintaining minimal ML.

When comparing the performance analysis of each filter element can deduce from Fig. 10 that the same trend holds for each varied velocities of 5 m/s and 10 m/s. This
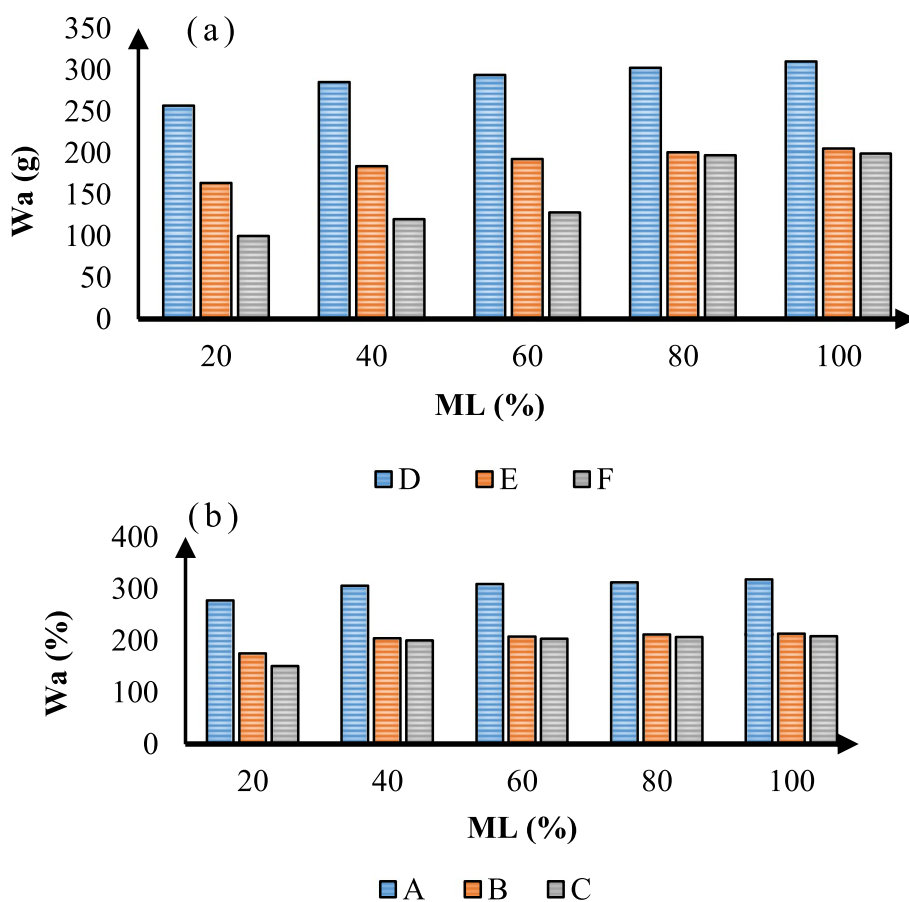
Effiom *et al. Journal of Engineering and Applied Science*   (2023) 70:131

Page 11 of 18

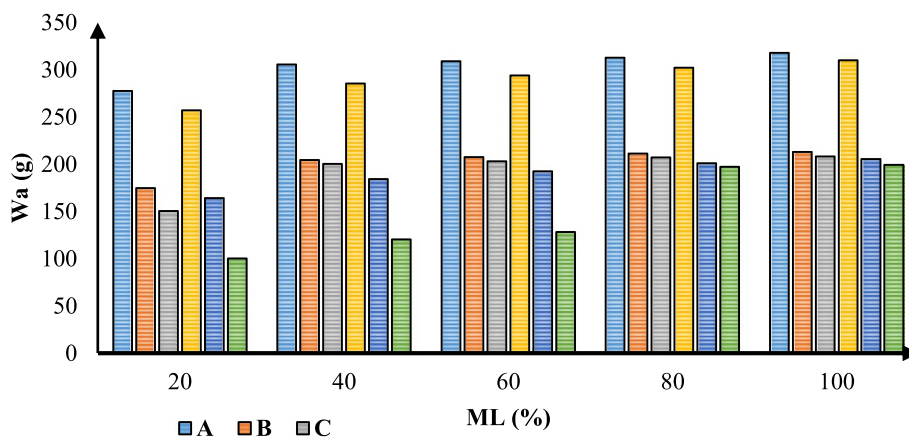**Fig. 9** **a** Mass accumulation @5 m/s and **b** mass accumulation @10 m/s

Fig. 10 Comparative mass concentration on filter elements

indicates that the first filter effectively removes particles from the airstream and can use pre-filters to remove large particles that contribute the most to filter loading [32]. Filter elements B, C, and E decreased the mass accumulation of 547.1 g, 493 g, 440 g and 340 g, respectively, when the filters were tested within 5 h of running time. From

[33], this phenomenon results from particulate matter distribution across the flow path with different sizes. This is in accordance with ASHRAE and EN-2022 standards for HVAC sample preparation of contaminant procedural testing. Furthermore, deposits and droplets were observed at the plenum area [34]. As noted by [33, 34], this could be due to several reasons, such as; clogging of media area, filter overloading, particle bombardment, and contaminant accumulation. According to [35], Accumulated mass flow on filter elements plays a significant role and determines the performance of the filter media, inlet parameters, and overall performance of the GT turbine system.

Effect of filtration efficiency across filter elements

The filter element performance was evaluated across stages of filtration housing as a function of the filter element's ability to remove particulate matter. It was determined based on the effectiveness of the filter to remove contaminants from the airstream. Figure 11 presents the result of filter efficiency across the filtration housing.

In Fig. 11, at 20% contaminant mass loading, all filter elements performed at their peak with filter efficiencies of 98.9%, 96.7%, 95.6% and 95.4% when compared with loaded filters A, B, C, D, E, and F (with contaminants). As mass loading increased with time, filter elements showed a decrease in filtration efficiencies (from 58.2 to 25.1%), signifying filters have reached their holding capacity, evident at all varied concentrations, which results in back pressure, thereby reducing the speed of the compressor of the filtration test rig. This is affirmed by [36] when studying the mathematical modelling of a multistage filtration system's trapezoidal shape. In a typical gas turbine operation under consideration, the effect could result in fouling, corrosion, surge, damage to the media face area, and high maintenance cost. In addition, maintaining a constant power supply may require more energy [37].

Relationship between accumulated mass (Wa) and pressure drop (Δp)

Variations in particulate matter distribution over the face area (FA) for a GT intake filtration system were enhanced by the experimental result from the test rig. In Fig. 12, the
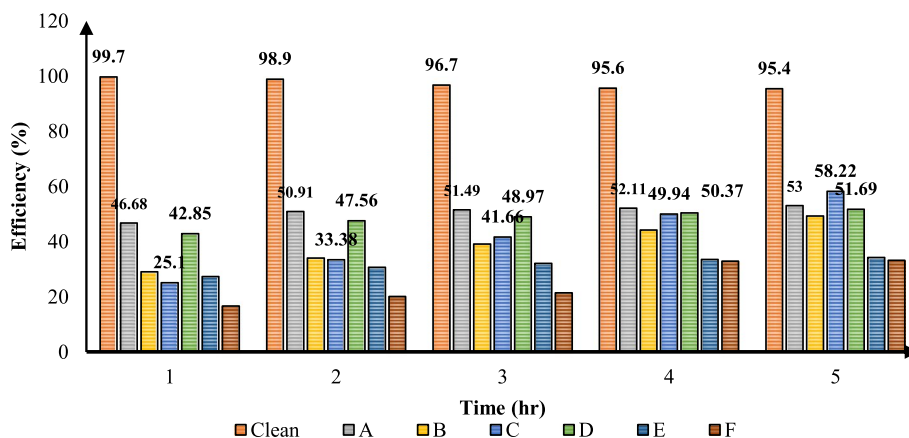

Fig. 11 Filter efficiency across filtration housing
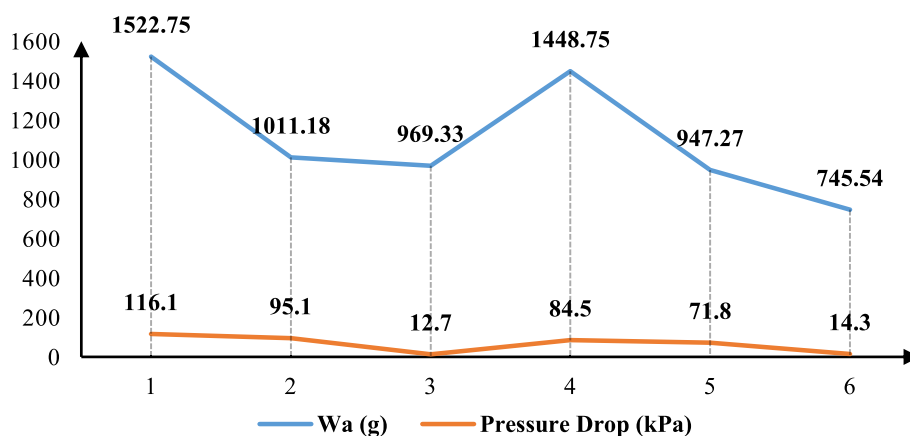
Fig. 12 Relationship between accumulated mass and pressure drop

relation indicated accumulated mass concentration on filter FA, which caused airflow resistance over individual filter elements.

The overall trend holds that at set-up velocities (10 m/s, 5 m/s), Filter A (1522.75 g), D (1448.75 g) and B (1011.18 g) elements at the first stage with higher accumulated mass, had higher differential pressures of 116.1 kPa, 84.5 kPa, and 95.1 kPa respectively across the housing. This is in comparison with filter elements C, E, and F, with less accumulation at 969.33 g, 947.27 g, and 745.54 g. Whereas filter element D deviated from the trend with a lower differential despite an increased mass higher than filter element B, attributed to possible variations in collective particle type and size distribution over filter surface area as well as clogging of filter media [5]. It is also observed that with increased velocity, shedding of accumulated mass over media occurred.

Relationship between filter flow rate (q) and pressure drop (Δp)

Figure 13 shows the relationship between pressure drop and filter flow rate at different velocities (10 m/s and 5 m/s, respectively). It can be established that the flow rate increases with increased pressure drop. According to [36], volumetric flow occurred in relation to filter resistance to airflow, thus preventing foulant from entering the engine. This could have a negative impact on the media area, thus, resulting in an increase in clogging and compressor work.

The filter resistance to airflow at 1.05 kPa to 6.18 kPa was recorded across filter housing. This trend continued throughout the stages of filtration housing.

Relationship between accumulated mass (Wa) and filtration efficiency (η)

The result obtained at different ML levels, filter elements A, D, E, and F, showed a linear relationship with different efficiencies resulting from particle deposition on elements (Fig. 14). Filter B and C demonstrated a non-linear relation resulting from the arrangement on the filtration housing. In a typical gas turbine operation, as contaminants are distributed within surrounding installations when filters become loaded, this may pose challenges to operators and affect the overall performance of the GT system. Maintenance cultures have been employed in this regard to reduce the impacts.
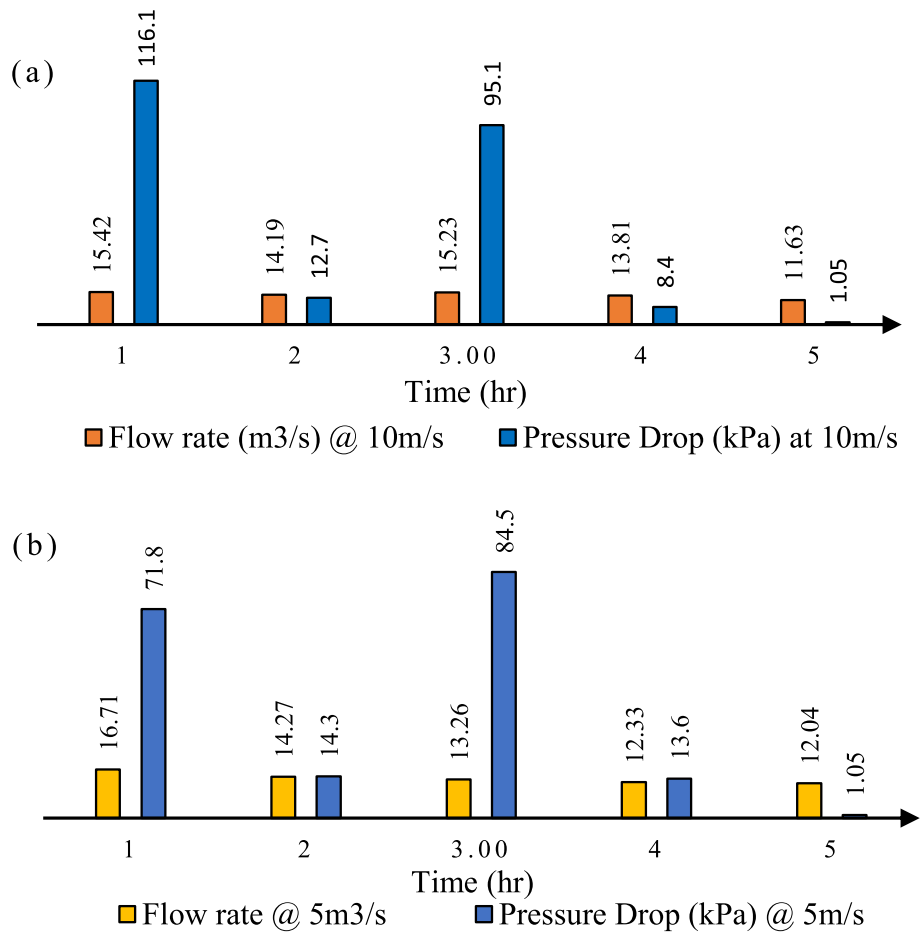
(a)

Flow rate (m3/s) @ 10m/s   Pressure Drop (kPa) at 10m/s

(b)

Flow rate @ 5m3/s   Pressure Drop (kPa) @ 5m/s

Fig. 13 Overall relationship between pressure drop and filter flow rate **a** 10 m³/s and **b** at 5 m³/s
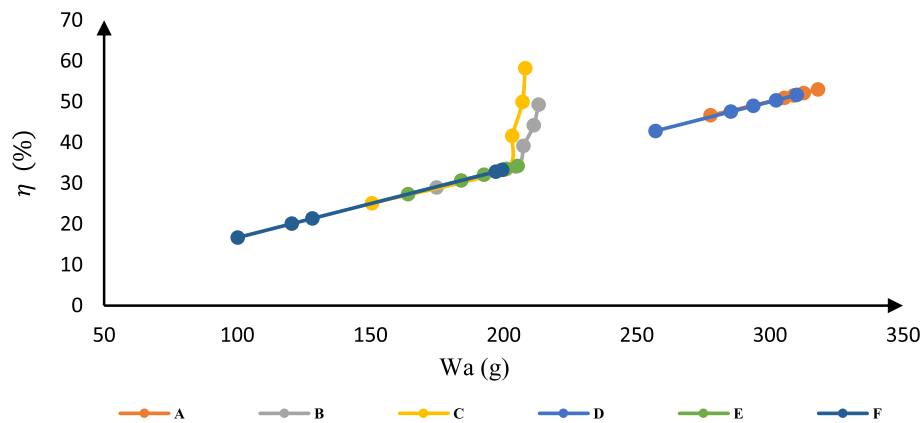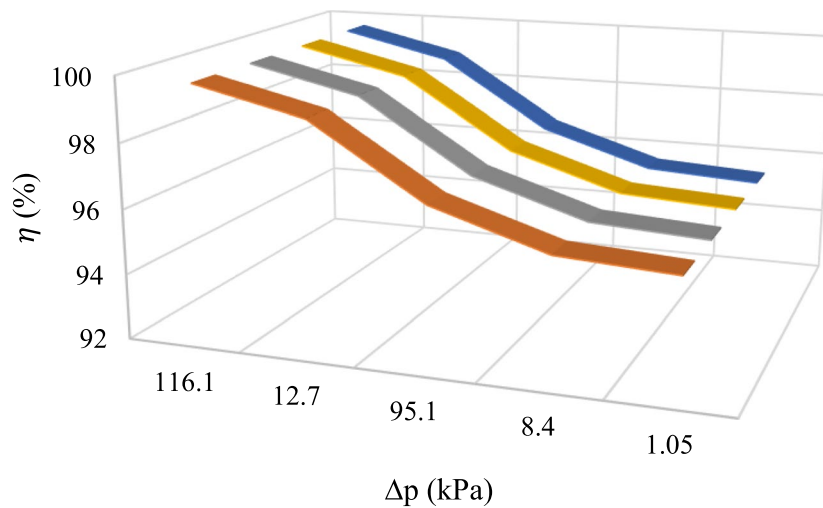

Fig. 14 Relationship between filtration efficiency (η) and mass accumulation (W_a)

Effect of pressure drop (Δp) on filtration efficiency (η)

Figure 15 shows the overall relationship between pressure drop and the efficiency of filter elements. As filter media accumulates particulate matter across filter housing, a significant change occurred between performance indicators. When evaluated, the

Fig. 15 Relationship between overall pressure drop and efficiency of filter elements

overall result of pressure drops and filtration efficiency showed that the total pressure differential amounted to 116.1 kPa (at 10 m/s) and 71.8 kPa (at 5 m/s). This may be due to the high resistance of particulate matter accumulating on media faces against airflow between the input and output faces of filter housing [38]. Therefore, it can be deduced that the relationship between efficiency and pressure differential is non-linear. This further indicates the distribution of particles across the airstream channel as contaminants' sizes intercept with filter media.

Experimental result validation

Comparison of summarised test results recorded at housing intake (Hi) to housing outlet (H_o), with literature for total differential pressure (ΔP_t), change in volumetric flow rates (ΔQ_f), and change in the sensible capacity of the compressor ($\Delta \Psi_s$) is presented in Table 2. This result was validated by the literature of [31, 27, 32, and 40] and conforms to the filtration flow phenomena. The increase in pressure differential resulted in a loss in the compressor's sensible capacity and a decrease in flow rate. The consequences may be huge, considering that industrial GT plants rely so much on the filtration system to enhance their health, performance, and life.

Table 2 Validation of result with literature

Outlet–inlet	Present study @ 10 m/s	Present study @ 5 m/s	[24]	[26]	[31]	[39]
ΔP_t (kPa)	101.80	58.20	215.00	1651.4	30.9	50
ΔQ_f (m³/s)	− 0.83	− 0.22	− 0.05	− 10	− 450	− 123
$\Delta \Psi_s$ (kW)	− 22.29	− 6.08	− 7.73	− 7.73	− 3	− 330

Conclusions

The analysis and results obtained from the study suggest that this methodology is promising in simulating offshore contaminant loading to select the best GT filtration system. The investigation made the following conclusions: The evaluated pressure drop for filters A–B, D–E, B–C and E–F across the housing were 19.02 kPa, 16.9 kPa, 2.54 kPa, and 2.86 kPa. However, an intake to outlet housing (Hi-Ho) pressure drop was 2.25 kPa. Accumulated mass across filter elements A, B, C. D, E, and F face area at the end of condition monitoring (20–100%) were 318.02 g, 213.14 g, 208.13 g, 310.15 g, 205.36 g, and 199.5 g, respectively. The efficiency of filter elements evaluated for the overall filter loading condition (20–100%) was A (53%), B (49.28%), C (58.22%), D (51.69%), E (34.23%), and F (33.25%). Across the varied filter elements B–C and E–F corresponding with filter class H12–E11 and G5–F9, a minimal pressure drop at 2.54 kPa, and 2.86 kPa, with compressor performance improvement of 22% and 31%, respectively. The results showed the effect of pressure drop, accumulated mass of filter element, and filter flow rate affect the filtration system and compressor performance. These results could aid GT users in deciding on filtration system selection, maintenance, and replacement procedures. In the study location, a 3-stage filtration combination of filter elements A–B, B–C, and D–E corresponding with filter class F7–H12, H12–E11, and E10–G5 was recommended for the GT filtration system having effectiveness at 51.14%, 53.75%, and 43% respectively.

Abbreviations

P_i	Inlet pressure (kPa)
P_e	Exit pressure (kPa)
P_t	Total pressure (kPa)
P_s	Static pressure (kPa)
W_a	Mass accumulation (kg)
ΔP_t	Total differential pressure (kPa)
W_m	Measured mass (kg)
q_s	Sensible capacity
Q_f	Volumetric flow rate (m³/s)

Authors' contributions
All authors contributed equally to this research, from conception to the final stages. All the authors read and ratified the completed manuscript.

Availability of data and materials
Data will be made available on request.

Declarations

Competing interests
The authors declare that they have no competing interests.

References
1.   De Castro-Cros M, Velasco M, Angulo C (2021) Machine-learning-based condition assessment of gas turbines - a review. Energies 14(24):8468. https://doi.org/10.3390/en14248468

Effiom *et al. Journal of Engineering and Applied Science*   (2023) 70:131

Page 17 of 18

2. Ezzat MF, Dincer I (2019) Development and exergetic assessment of a new hybrid vehicle incorporating gas turbine as powering option. Energy 170:112–119. https://doi.org/10.1016/j.energy.2018.12.141

3. Oyedepo SO, Fagbenle RO, Adefila SS, Adavbiele SA (2014) Performance evaluation and economic analysis of a gas turbine power plant in Nigeria. Energy Convers Manage 79:431–440. https://doi.org/10.1016/j.enconman.2013.12.034

4. Igie DA, Michailidis G, Minervino O (2016) Performance of inlet filtration system in relation to the uncaptured particles causing fouling in the gas turbine compressor. J Eng Gas Turbine Power 138:012601. https://doi.org/10.1115/1.4031223

5. Brekken OL, and Syverud E (2009) Filtration of gas turbine intake air in offshore installations: the gap between test standards and actual operating conditions. In Turbo Expo: Power for Land, Sea, and Air, vol.48869,pp.371-379 https://doi.org/10.1115/GT2009-59202

6. Fentaye AD, Aklilu TB, Syed IG, Konstantinos Kyprianidis G (2019) A review on gas turbine gas-path diagnostics: State-of-the-art methods, challenges and opportunities. Aerospace 6(7):83. https://doi.org/10.3390/aerospace6070083

7. Marwaha G, and Joshua K (2019) Predictive Maintenance of Gas Turbine Air Inlet Systems for Enhanced Profitability as a Function of Environmental Conditions. In Abu Dhabi International Petroleum Exhibition & Conference .OnePetro. https://doi.org/10.2118/197814-MS

8. Madsen S, and Lars EB (2018) Gas turbine fouling offshore: Effective online water wash through high water-to-air ratio. In Turbo Expo: Power for Land, Sea, and Air, vol. 51180. American Society of Mechanical Engineers. p.V009T27A016. https://doi.org/10.1115/GT2018-75618

9. Rath N, Mishra RK, Abhijit K (2022) Aero engine health monitoring, diagnostics and prognostics for condition-based maintenance: An overview. Int J Turbo Jet-Engines. https://doi.org/10.1515/tjeng-2022-0020

10. Madsen S, and Lars EB (2014) Gas turbine operation offshore: On-line compressor wash operational experience. In Turbo Expo: Power for Land, Sea, and Air, vol. 45660. American Society of Mechanical Engineers, p. V03BT25A008 https://doi.org/10.1115/GT2014-25272

11. Abdul-Wahab SA, Omer ASM, Yetilmezsoy K, Bahramian M (2020) Modelling the clogging of gas turbine filter houses in heavy-duty power generation systems. Math Comput Model Dyn Syst 26(2):119–143. https://doi.org/10.1080/13873954.2020.1713821

12. Purba O, Zhultriza F (2021) Gas Turbine Hidden Capacity Recovery by Inlet Air Filter Variation Method to Produce Clean and Efficient Energy. In: IOP Conference Series: Materials Science and Engineering, vol.1096,no.1. IOP Publishing, p. 012089. https://doi.org/10.1088/1757-899X/1096/1/012089.

13. Aldi N, Casari N, Dainese D, Morini M, Pinelli M, Spina P , & Suman A (2017 June). The effects of third substances at the particle/surface interface in compressor fouling. In Turbo Expo: Power for Land, Sea, and Air, Vol. 50961, American Society of Mechanical Engineers, p. V009T27A019. https://doi.org/10.1115/GT2017-64425

14. Purba O, and Zhultriza F (2021). Gas Turbine Hidden Capacity Recovery by Inlet Air Filter Variation Method to Produce Clean and Efficient Energy. IOP Conference Series: Materials Science and Engineering. Vol.1096.No1. IOP Publishing, https://doi.org/10.1088/1757-899X/1096/1/012089

15. Swain B, Mallick P, Patel S, Roshan R, Mohapatra SS, Bhuyan S, Priyadarshini Behera MBSS, Behera A (2020) Failure analysis and materials development of gas turbine blades. Mater Today Proc 33:5143–5146. https://doi.org/10.1016/j.matpr.2020.02.859

16. Zhang P, Gao Z, Cao L, Dong F, Zou Y, Wang K, Sun P (2022) Marine systems and equipment prognostics and health management: a systematic review from health condition monitoring to maintenance strategy. Machines 10(2):72. https://doi.org/10.3390/machines10020072

17. Liu Y, Banerjee A, Ravichandran T, Kumar A, Heppler G (2018) Data analytics for performance monitoring of gas turbine engine. Annual conference of the prognostics and health management society, p 1–9. https://doi.org/10.36001/phmconf.2018.v10i1.470

18. Hanachi H, Liu J, Banerjee A, Chen Y (2015) A framework with nonlinear system model and nonparametric noise for gas turbine degradation state estimation. Meas Sci Technol 26(6):065604. https://doi.org/10.1088/0957-0233/26/6/065604

19. Auda SA, & Ali OM (2023). Effect of operating conditions and air filters maintenance on the performance and efficiency of gas turbine power plant. Materials Today: Proceedings. https://doi.org/10.1016/j.matpr.2023.01.290

20. Tian X, Ou Q, Pei C, Li Z, Liu J, Liang Y, Pui DY (2021) Effect of main-stage filter media selection on the loading performance of a two-stage filtration system. Build Environ 195:107745. https://doi.org/10.1016/j.buildenv.2021.107745

21. ISO 16890-1:2016 (en), Air filters for general ventilation- Part 1: Technical specifications, requirements and classification system based upon particulate matter efficiency (ePM). https://www.iso.org/standard/57864.htm

22. Li X, and Xin T (2018). Optimisation of gas Turbine Filtration System based on Life Cycle Cost LCC Theory. In 2017 3rd International Forum on Energy, Environment Science and Materials (IFEESM 2017). Atlantis Press, pp. 997–1006. https://doi.org/10.2991/ifeesm-17.2018.185

23. Tahan M, Tsoutsanis E, Muhammad M, Karim ZA (2017) Performance-based health monitoring, diagnostics and prognostics for condition-based maintenance of gas turbines: a review. Appl Energy 198:122–144. https://doi.org/10.1016/j.apenergy.2017.04.048

24. Kruger A J (2013). The impact of filter loading on residential hvac performance (Doctoral dissertation, Georgia Institute of Technology). http://hdl.handle.net/1853/50344

25. Tadeusz D, Mirosław K (2022) Experimental study of the effect of air filter pressure drop on internal combustion engine performance. Energies 15:3285. https://doi.org/10.3390/en15093285

26. Abam FI, Effiom SO, Ohunakin OS (2016) CFD evaluation of pressure drop across a 3-D filter housing for industrial gas turbine plants. Front Energy 10:192–202. https://doi.org/10.1007/s11708-016-0406-x

27. Mohammed AS, Zaytoon MHH, Yiyun LX (2021) Generalised models of flow of a fluid with pressure-dependent viscosity through porous channels: channel entry conditions. Int J Phys Res 9(2):84–91

28. Vecherkovskaya A. and Popereshnyak S. (2017). Mathematical Modeling of the Process of Fluid Filtration through a Multi-layer Filtering element. Measuring Methods in Chemical industry. UDC 66.067.22:004.021 https://doi.org/10.15587/2312-8372.2017.109309

29. Hanachi H, Liu J, Banerjee A, Chen Y, Koul A (2014) A physics-based modeling approach for performance monitoring in gas turbine engines. IEEE Trans Reliab 64(1):197–205

30. Hiner S D (2011). Strategy for selecting optimised technologies for gas turbine air inlet filtration systems. In Turbo Expo: Power for Land, Sea, and Air, vol. 54648, pp. 559-568 https://doi.org/10.1115/GT2011-45225

31. Stephen B, Novoselac A, Siegel JA (2010) The effects of filtration on pressure drop and energy consumption on residential HVAC systems. HVAC and Research 16(3):273–294

32. Effiom SO, Abam FI, Ohunakin OS (2015) Performance modeling of industrial gas turbines with inlet air filtration system. Case Stud Thermal Eng 5:160–167. https://doi.org/10.1016/j.csite.2015.03.008

33. Wilcox M, Kurz R, & Brun K (2011). Successful selection and operation of gas turbine inlet filtration systems. In Proceedings of the 40th Turbomachinery Symposium. Texas A&M University. Turbomachinery Laboratories. https://doi.org/10.21423/R1RD20

34. Wilcox M, Kurz R, Brun K (2012) Technology review of modern gas turbine inlet filtration systems. Int J Rotating Mach. https://doi.org/10.1155/2012/128134

35. Vulpio SA, Casari N, Pinelli M (2021) Dust ingestion in a rotorcraft engine compressor: Experimental and numerical study of the fouling rate. Aerospace 8(3):81. https://doi.org/10.3390/aerospace8030081

36. Kurz R, Orhon D, Hiner S, & Benson J (2015). Gas Turbine Air Filtration Systems For Offshore Applications. In Proceedings of the 44th Turbomachinery Symposium. Turbomachinery Laboratories, Texas A&M Engineering Experiment Station. https://doi.org/10.21423/R1Q62M

37. Robb D (2020). Better Filtration= Better Performance: Inlet air filtration in gas turbine performance and efficiency. Turbomachinery Magazine. https://www.turbomachinerymag.com

38. Schirmeister U. and Mohr F (2016 June). Impact of enhanced GT air filtration on power output and compressor efficiency degradation. In Turbo Expo: Power for Land, Sea, and Air, Vol.49743. American Society of Mechanical Engineers, p.V003T08A003 https://doi.org/10.1115/GT2016-56292

39. Nassif N (2012). The impact of air filter pressure drop on the performance of typical air-conditioning systems. In Building Simulation, Tsinghua Press,. 5, pp.345–350. https://doi.org/10.1007/s12273-012-0091-6

Publisher's Note